Robust Design of Trailing Edge Flap with Orthogonal Array Inspired Response Surface for Helicopter Vibration Reduction

Rajnish Mallick[1], Ranjan Ganguli[2], M. Seetharama Bhat[3]

[1, 2, 3] Department of Aerospace Engineering, Indian Institute of Science, Bangalore 560012, India

Abstract

The robust design of helicopter rotor on-blade active trailing edge flaps is presented. In this study, we use optimization techniques to obtain the optimal spanwise and chordwise length of a single and dual trailing-edge flap. The objective of this study is to determine a robust design of trailing edge flap to achieve minimum hub vibration levels and minimize the requirement of flap actuation power. An aeroelastic analysis of a soft in-plane 4-bladed rotor similar to BO105 is performed in conjunction with an optimal control to minimize hub vibrations levels. A Pareto optimal design approach is used to obtain optimal design point for the mutually conflicting objectives. A Pareto optimal point reduces vibration levels by 71% and 72% from the baseline case, while reducing flap actuation power by 17% and 20%, in comparison to the initial design for single and dual flap case, respectively. It is found that second order polynomial response surface based on Taguchi L_9 orthogonal array (OA) with 3-level design describes both the objectives adequately.

1. INTRODUCTION

Rotor induced helicopter vibration reduction is still a challenging area of research in helicopter dynamics. Severe vibration levels in helicopter pose a challenge to develop passenger/pilot friendly helicopter cabins. In forward flight, helicopter experiences highly asymmetric lift distribution over the rotor disc, which rotates in an unsteady aerodynamic environment resulting in high vibratory loads at the hub[1-2]. High vibration levels lead to crew and passenger discomfort, affects avionics, decrease fatigue life of the various structural components and hence lead to increase in the maintenance costs. Passive vibration control devices such as vibration isolators or vibration absorbers are used to suppress the vibratory loads at the selected places in the helicopter body. But passive devices incurs large weight penalty and their performance degrades from the tuned flight condition [3].

With the advent of smart materials, active vibration control techniques have caught attention of researchers[4-5]. In the last two decades, various active approaches were tested numerically[4,6-7] and experimentally[8-10]. Piezo actuated active control flap (ACF) method have emerged as the best potential candidate to alleviate helicopter vibration[10-12]. Figures 1 and 2 show the schematic of the single and dual trailing edge flaps. Some studies show that multiple trailing edge flaps (TEFs) are capable of achieving better vibration reduction in comparison to single TEF[13]. Most of the studies available in literature use parametric studies to find the best design for trailing edge flaps[14]. However, an active method incurs high cost and has reliability issues.

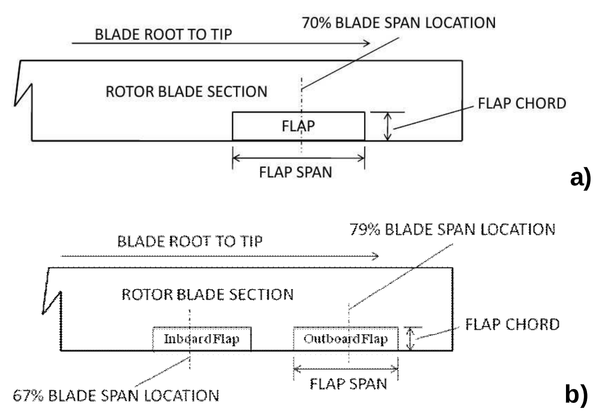

Figure 1. Schematic view of rotor blade with **a)** single trailing edge flap **b)** dual trailing edge flap

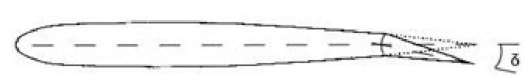

Figure 2. Outline of the cross-section of deflected trailing edge flap (Side View)

Several researchers sought to reduce helicopter vibration levels by an alternative approach by designing a low vibration rotor using optimization method[15-18]. Various design variables such as blade mass, stiffness distribution, advanced blade geometry were studied thoroughly to minimize the vibratory hub loads. Some studies focused on rotor

[1] Ph.D. student, rajnish@aero.iisc.ernet.in
[2] Professor, ganguli@aero.iisc.ernet.in
[3] Professor, msbdcl@aero.iisc.ernet.in

optimization using gradient based optimization method[19]. Some researchers have used analytical derivatives to reduce the computational time for rotor optimization[17,20]. Ganguli[21] presents a review on the use of optimization in helicopter engineering. Integration of optimization algorithms with computationally intensive simulation codes often used in helicopter engineering poses an even greater challenge as it leads to high computational costs. This problem can be resolved by use of inexpensive metamodels or surrogates, replacing the expensive computer analysis codes.

Metamodeling techniques are widely used in multidisciplinary design optimization problems[22-24]. Response surface method (RSM) is one such metamodeling technique which is widely used in various structural optimization problems[25-27]. Response surface method gives global approximations in contrast to Taylor series which yield only local approximations. Myers and Montgomery present an excellent introduction to RSM[28]. But only few studies on RSM have been conducted for helicopter optimization[27,29-30]. Ganguli[31] used response surfaces for helicopter optimization and successfully demonstrated the decoupling of the structural design problem and the optimization problem. Response surfaces are polynomial approximations to the design analysis problem. A low computational cost is involved for using RSM, nevertheless there is one disadvantage with response surface method based on design of experiments (DOE). As the number of design variables increases, the computational cost for RSM goes up exponentially. This problem can be ameliorated by use of orthogonal arrays (OAs).

Orthogonal arrays are simple fractional factorial designs and are used widely in higher dimensional problems for sparse experimental trials. OAs have been extensively used for quality control[32] and parametric optimization[33]. Some researchers have used OA in conjunction with RSM to construct response surfaces for optimization studies[26-27,34]. Hu et.al [33] developed a robust design method for horizontal axis wind turbines using OAs.

In this study, we develop orthogonal array inspired response surfaces for robust design of trailing edge flaps for helicopter vibration alleviation. An optimal control algorithm is used to determine the flap angles. Aeroelastic analysis is used to predict the reduced hub loads. The objective is to minimize the rotor induced vibration and power required for flap actuation. Note that this robust optimization technique can be used for various other complex rotor design problems in helicopter industry. This study will introduce a robust design approach for developing active trailing edge flaps.

2. AEROELASTIC ANALYSIS

The aeroelastic analysis used in this study is discussed below briefly. Details of the analysis are available in earlier papers[31,35]. The formulation is based on the generalized Hamilton's principle applicable to non-conservative systems.

(1) $$\int_{\psi_1}^{\psi_2} (\delta U - \delta T - \delta W)\, d\psi = 0$$

Here δU , δT and δW are the virtual strain energy, kinetic energy and work, respectively. Governing equations of motions are discretized using finite element method. The aerodynamic forces and moments acting on the blade section are calculated under forward flight condition. Air loads due to rotor blade motion and trailing edge flap deflections are predicted using Hariharan and Leishman unsteady aerodynamic model[36]. The resulting nonlinear ODEs in time are transformed into the normal mode space and solved for the steady-state blade response using the finite element in time procedure. The key finite element equation after normal mode transformation is:

(2) $$M\ddot{p}(\psi) + C\dot{p}(\psi) + Kp(\psi) - F(p, \dot{p}, \psi) = 0$$

Here M , C and K are the normal mode mass matrix, damping matrix and stiffness matrix, respectively. Also, F is the force vector and p represents the modal displacement vector. The blade azimuth angle is denoted by ψ . Once the steady state blade response is determined, the loads acting at the rotor hub are calculated by summing the contributions of individual blades at the root. A coupled trim procedure is followed to find the blade response, pilot input control angles Θ and orientation of the vehicle, simultaneously. The coupled trim equation is:

(3) $$F(\Theta) = 0$$

For a N_b bladed helicopter rotor with identical blades, the dominant component of hub vibratory loads is the $N_b\Omega$ harmonic, which is transmitted to the airframe. This aeroelastic model has been validated with wind tunnel data[37] and flight test data[38].

3. CONTROL ALGORITHM

In the present study, trailing-edge flap is deflected at higher harmonics of the rotor rotational speed. A careful phasing of the trailing-edge flap motion can create new unsteady aerodynamic loads which cancel the original vibratory loads at the rotor hub.

Typically, for a N_b-bladed rotor, the flaps are deflected at $N_b - 1/rev$, N_b / rev and $N_b + 1/rev$ harmonics of the rotor rotational speed. The multi-harmonic control law for the TEF can be written as:

$$\delta(\psi) = \delta^{3c}\cos(3\psi) + \delta^{3s}\sin(3\psi) + \delta^{4c}\cos(4\psi) + \delta^{4s}\sin(4\psi) + \delta^{5c}\cos(5\psi) + \delta^{5s}\sin(5\psi) \quad (4)$$

The above six unknown flap harmonics are obtained using an optimal control algorithm[14,39]. The algorithm is based on the minimization of,

$$J_v = \mathbf{Z}^T \mathbf{W}_z \mathbf{Z} + \mathbf{u}^T \mathbf{W}_u \mathbf{u} \quad (5)$$

Where $\mathbf{Z}$ contains the 4/rev hub vibratory loads and $\mathbf{u}$ contains the flap control harmonics. The second term in Eq. (5) is introduced to keep the required control input (flap angles) within practically achievable limits. Here $\mathbf{Z}$ is the hub vibratory load vector containing the N_b / rev sine and cosine harmonics.

$$\mathbf{Z} = \begin{bmatrix} F_{xH}^{4P} & F_{yH}^{4P} & F_{zH}^{4P} & M_{xH}^{4P} & M_{yH}^{4P} & M_{zH}^{4P} \end{bmatrix}^T \quad (6)$$

$$\mathbf{u} = \begin{bmatrix} \delta^{3c} & \delta^{3s} & \delta^{4c} & \delta^{4s} & \delta^{5c} & \delta^{5s} \end{bmatrix}^T \quad (7)$$

Either hub shears or moments can be reduced by suitably modifying the weighting matrix $\mathbf{W}_z$ in Eq. (5). In the current study, all hub shears and moments are weighted equally. A global controller is used to determine the optimal control input[39]. The first order Taylor series expansion about the zero control input (no trailing-edge flap motion) is evaluated. The hub load vector $\mathbf{Z}$ is related to the control inputs using a transfer matrix. Linearizing the system about the control inputs using Taylor's series expansion gives,

$$\mathbf{Z} = \mathbf{Z}_0 + \mathbf{T}\mathbf{u} \quad (8)$$

Here $\mathbf{T}$ is the transfer matrix that relates the system response to motion of the trailing edge flap. This transfer matrix is assumed to be constant over the entire range of the control input. Transfer matrix is calculated only once by perturbing the control harmonics individually around zero control inputs. Eq. (8) is substituted into eq. (5), and then the following optimality criteria is applied,

$$\frac{\partial J_v}{\partial \mathbf{u}} = 0 \quad (9)$$

Thus the optimal controller becomes,

$$\tilde{\mathbf{u}} = \mathbf{C}\mathbf{Z}_0 - \mathbf{C}\mathbf{T}\mathbf{u} \quad (10)$$

$$\mathbf{C} = -\mathbf{D}\mathbf{T}^T \mathbf{W}_Z \quad (11)$$

$$\mathbf{D} = (\mathbf{T}^T \mathbf{W}_Z \mathbf{T} + \mathbf{u})^{-1} \quad (12)$$

Here $\tilde{\mathbf{u}}$ represents the optimal control inputs obtained from the controller.

The power required by the flap actuation system is obtained by integrating the product of the hinge moment and flap deflection over the azimuth. Note that the instantaneous power required at the flap hinge, $-M_h \overset{*}{\delta}$, may be negative over some portions of the azimuth. Typically the actuator is unable to transfer the power back to its power supply. Therefore, the net flap actuation power (J_P) can be written as follows[7, 30]:

$$J_p = \frac{N_b}{2\pi} \int_0^{2\pi} \max(-M_h \overset{*}{\delta}, 0) \delta\psi \quad (13)$$

4. OPTIMIZATION PROBLEM

The objective of this investigation is to search an optimal design configuration for single and dual trailing edge flaps. The design variables in this study are flap chord and flap length. A robust optimization technique is used to achieve the objective of minimum vibration levels, simultaneously reducing the power required for actuating the flaps. Flaps are located at their optimal locations for vibration reduction objective function[30]. Midpoint of single TEF is located at 70%R from the blade root as shown in Figure 1a. Inboard and outboard flaps in dual flap configuration are located at 67%R and 79%R, respectively as shown in Figure 1b. Viswamurthy et.al [30] considered the placement of two flaps on the rotor blade. However, they did not consider the effect of flap geometry on the helicopter vibration levels and flap actuation power, which is the subject of present investigation using a robust design method. The values of J_v and J_P are normalized with respect to their corresponding baseline case (starting design point, S). These normalized values are denoted by F_v and F_P, respectively. The optimization problem is formulated as follows:

(14) Minimize $\{F_v^j, F_P^j\}; j = SF, DF$

(15) Subject to:

$$\left.\begin{array}{l} x_{1,lower} \le x_1 \le x_{1,upper} \\ x_{2,lower} \le x_2 \le x_{2,upper} \end{array}\right\} SingleFlap(SF)$$

$$\left.\begin{array}{l} y_{1,lower} \le y_1 \le y_{1,upper} \\ y_{2,lower} \le y_2 \le y_{2,upper} \end{array}\right\} DualFlap(DF)$$

In dual flap case, both the flaps have the same dimensions. The objective functions are of conflicting nature for the same choice of design variables. Trying to obtain a high level of vibration reduction needs a high level of flap power. This kind of optimization problems falls under the category of multi-objective design optimization. The trade-off between the objectives depends on the nature of the Pareto curve, which is obtained by plotting both the objectives with respect to each other in a 2D plane. An optimization solution is said to be Pareto optimal if it impossible to minimize one objective without increasing the other objectives. A response surface method (RSM) is used to obtain metamodels of the objective function in terms of second order polynomials. The optimization problem is decoupled from the expensive aeroelastic analysis using RSM. Therefore, these low order polynomial approximations will serve as an objective functions which can be easily evaluated for Pareto optimal design points.

5. RESPONSE SURFACE METHOD

Response surface methods (RSM) are a collection of statistical and mathematical techniques which are used for improving and optimizing products and processes. RSM generates a functional relation between an output variable and set of input variables (independent variables)[28,40] :

(16) $y = f(x) + \varepsilon$

Here f is an unknown function and ε represents the error in the approximation. In RSM approach, the error ε is treated as a statistical error, with zero nominal distribution, zero mean and variance σ^2. The relationship between input variables and output (response) is obtained using a low number of design experiments using Taguchi orthogonal arrays. Response surfaces are smooth analytical functions that are usually approximated with second order polynomials. The second order model captures the curvature and interaction effects along with the slope. A second order response surface is obtained by a linear regression technique to approximate the objective functions. For instance, a general second order polynomial response surface is shown as follows:

(17)

$$y(x_i) = \beta_0 + \sum_{i=1}^{k} \beta_i x_i + \sum_{i=1}^{k} \beta_{ii} x_i^2 + \sum_{i<j}^{k} \sum_{j}^{k} \beta_{ij} x_i x_j + \varepsilon$$

A response surface for two design variables is shown as:

(18)

$$y(x_1, x_2) = \beta_0 + \beta_1 x_1 + \beta_2 x_2 + \beta_{11} x_1^2 + \beta_{22} x_2^2 + \beta_{12} x_1 x_2 + \varepsilon$$

Here, y is the response surface obtained from the input variables x_1 and x_2.

Parameters $\beta_0, \beta_i, \beta_{ii}$ and β_{ij} in eq.17 are the regression coefficients obtained by using regression analysis. The method of least squares is invoked to estimate the regression coefficients, which minimizes the sum of the squares of the deviation of the predicted values $\hat{y}(x)$, from the actual values $y(x)$. To obtain parameters $\beta's$, eq. 17 and 18 can be written as:

(19) $\mathbf{y} = \mathbf{X}\beta + \varepsilon$

Here $\mathbf{y}$ and ε are n x 1 vectors of responses and errors terms, respectively, β is a k x 1 vector of regression coefficients, $\mathbf{X}$ is an n x k matrix of sample data points with k as number of design points. We can write,

(20) $\mathbf{y} = [y_1, y_2, \ldots, y_n]^T$

(21) $\beta = [\beta_0, \beta_1, \ldots, \beta_k]^T$

(22) $\varepsilon = [\varepsilon_1, \varepsilon_2, \ldots, \varepsilon_n]^T$

and,

(23) $$\mathbf{X} = \begin{bmatrix} 1 & x_{11} & x_{12} & x_{11}^2 & x_{12}^2 & x_{11}x_{12} \\ 1 & x_{21} & x_{22} & x_{21}^2 & x_{22}^2 & x_{21}x_{22} \\ \vdots & \vdots & \vdots & \vdots & \vdots & \vdots \\ 1 & x_{n1} & x_{n2} & x_{n1}^2 & x_{n2}^2 & x_{n1}x_{n2} \end{bmatrix}$$

The parameters $\beta_0, \beta_i, \beta_{ii}$ and β_{ij} are obtained by minimizing the least square error obtained using the following relation[40]:

(24) $$L = \sum_{i=1}^{n} \varepsilon_i^2 = \varepsilon^T \varepsilon = (\mathbf{y} - \mathbf{X}\beta)^T (\mathbf{y} - \mathbf{X}\beta)$$

(25) $$L = \mathbf{y}^T \mathbf{y} - 2\beta^T \mathbf{X}^T \mathbf{y} + \beta^T \mathbf{X}^T \mathbf{X}\beta$$

To find the optimal value of the regression coefficients β, set

(26) $$\left.\frac{\partial L}{\partial \beta}\right|_{\hat{\beta}} = -2\mathbf{X}^T \mathbf{y} + 2\mathbf{X}^T \mathbf{X}\hat{\beta} = 0$$

Solving eq. 26 gives,

(27) $$\hat{\beta} = (\mathbf{X}^T \mathbf{X})^{-1} \mathbf{X}^T \mathbf{y}$$

Therefore, the fitted regression model is:

(28) $$\hat{y}(x) = \mathbf{X}\hat{\beta}$$

6. Taguchi Orthogonal Array

In the present study, the Taguchi L_9 orthogonal array is used to sparsely construct experimental design points required for generation of response surfaces. Orthogonal arrays (OAs) provide a systematic approach to perform numerical experiments with a fraction of designs points for the factorial design[41-42]. Fractional factorial experimental design use only a fraction of the total number of possible combinations to estimate the main effects and interactions. Here, orthogonality implies that the factors can be evaluated independent of each other[40-42]. A L_9 OA for 3-level design is shown in Table 1. The values -1,0 and 1 in the table correspond to the three levels of the variable. Note that the columns corresponding to the design variables in Table 1 are orthogonal. In general form, for an orthogonal array,

$$\mathbf{X}_{OA} = [x_1, x_2 \cdots, x_n],$$

$$x_i^T x_j = 0; i \neq j.$$

Since two columns are independent, their effect on the response can be evaluated independently of each other.

Table 1: 3-level L_9 orthogonal array

	Design Variables	
Point	x_1	x_2
1	1	1
2	1	-1
3	-1	-1
4	-1	1
5	0	0
6	0	1
7	1	0
8	-1	0
9	0	-1

Evaluations of J_v and J_P for the coded and physical values of the design variables for single and dual flap configurations are shown in Table 2 through Table 5, respectively.

Table 2: J_v at coded and physical values for single flap configuration

Coded values	**Length** x_1	**-1**	**0**	**1**
Chord x_2	Physical values	**4%**	**8%**	**12%**
-1	**10%**	5.91E-06	4.12E-06	3.67E-06
0	**15%**	5.64E-06	3.97E-06	3.63E-06
1	**20%**	5.61E-06	3.92E-06	3.62E-06

Table 3: J_P at coded and physical values for single flap configuration

Coded values	**Length** x_1	**-1**	**0**	**1**
Chord x_2	Physical values	**4%**	**8%**	**12%**
-1	**10%**	3.169E-08	4.65E-08	5.28E-08
0	**15%**	4.557E-08	6.36E-08	7.18E-08
1	**20%**	6.11E-08	8.34E-08	9.62E-08

The starting design point for single flap is with flap length of 8%R and flap chord of 0.15. The initial flap design parameters for inboard and outboard flap in dual flap case are 6%R flap length and 0.15 chord length. Both inboard and outboard flaps have same dimensions.

Table 4: J_v at coded and physical values for dual flap configuration

Coded values	Length y_1	-1	0	1
Chord y_2	Physical values	**4%_4%**	**6%_6%**	**10%_10%**
-1	**10%**	5.46E-06	4.12E-06	3.60E-06
0	**15%**	4.99E-06	3.93E-06	3.56E-06
1	**20%**	4.79E-06	3.87E-06	3.55E-06

Table 5: J_P at coded and physical values for dual flap configuration

Coded values	Length y_1	-1	0	1
Chord y_2	Physical values	**4%_4%**	**6%_6%**	**10%_10%**
-1	**10%**	3.98E-08	4.89E-08	5.50E-08
0	**15%**	5.73E-08	6.86E-08	7.70E-08
1	**20%**	7.76E-08	9.28E-08	1.10E-07

7. RESULTS AND DISCUSSION

In this study, numerical results are obtained for a 4-bladed, soft in-plane, uniform, hingeless rotor similar to the BO105 rotor. The baseline rotor and trailing edge flap properties are shown in Table 6. Move limits of design variables for physical and coded variables in design space are shown in Table 2 through Table 5. The flap chord and flap span for single flap varies from 0.10c to 0.20c and 4%R to 12%R, respectively. In dual flap case, both inboard and outboard flap chord and flap length varies from 0.10c to 0.20c and 4%R to 10%R, respectively. Here c represents the blade chord and R is the rotor blade radius. The largest flap span is constrained to 12%R for single flap and 10%R for dual flap, so that a single actuator assembly could be adequate enough to deflect the flap. Moreover, smallest flap length of 4%R is chosen to ensure that there is enough moment generation capacity of the flap to reduce hub loads[10].

7.1. Response Surfaces for Single and Multiple Flap Configurations

Objective functions F_v and F_P are evaluated at the data points generated through L_9 orthogonal array for 3 level design using helicopter aeroelastic analysis. The response surfaces determined using least square method for single and dual flap case are:

(29) $$F_v^{SF} = 0.9985 - 0.2620x_1 - 0.0230x_2 + 0.1706x_1^2 + 0.0165x_1x_2 + 0.0156x_2^2$$

(30) $$F_P^{SF} = 0.9970 + 0.2161x_1 + 0.2874x_2 - 0.0731x_1^2 + 0.0252x_1x_2 + 0.0552x_2^2$$

(31) $$F_v^{DF} = 0.9992 - 0.1918y_1 - 0.0412y_2 + 0.0892y_1^2 + 0.0168y_1y_2 + 0.0395y_2^2$$

(32) $$F_P^{DF} = 0.9923 + 0.1635y_1 + 0.3317y_2 - 0.0099y_1^2 + 0.0439y_1y_2 + 0.0623y_2^2$$

Table 6: Baseline blade and flap properties

Blade Properties	
N_b	4
c/R	0.055
Solidity, σ	0.07
Lock number, γ	5.20
C_T/σ	0.07
Blade pretwist	0.0
Precone, β_P	0.0
$EI_y / m_o\Omega^2R^4$	0.0108
$EI_z / m_o\Omega^2R^4$	0.0268
$GJ / m_o\Omega^2R^4$	0.00615
m_o, kg/m	6.46
Ω*, RPM*	383
R, m	4.94
Trailing-edge flap properties	
c_f / c	0.15
m_f / m_o	0.10
X_g^f / c_f	0.20

Tables 7 till Table 10 show the comparison of the response surface prediction and aeroelastic analysis at 9 different data points for two mutually contradicting objectives F_v and F_P, for single and dual flap case, respectively. Note that F_v is predicted by the response surface within an error limit of less than 1% for single flap case. While maximum variation between the predicted and the aeroelastic analysis is around 7%.

Table 7: F_v for RSM for single flap with MH input with 2nd order fit using L_9 OA

x_1	x_2	x_1^2	x_2^2	$x_1 * x_2$	J_v Analysis Prediction	Analysis Dimensionless w.r.t baseline	F_v RSM Prediction (second order fit)	Error b/w RSM (2nd order fit) and Analysis prediction (%)
1	1	1	1	1	3.62E-06	0.9130	0.9161	0.34
1	-1	1	1	-1	3.67E-06	0.9261	0.9292	0.33
-1	-1	1	1	1	5.91E-06	1.4900	1.4862	-0.26
-1	1	1	1	-1	5.61E-06	1.4146	1.4072	-0.53
0	0	0	0	0	3.97E-06	1.0000	0.9985	-0.15
0	1	0	1	0	3.92E-06	0.9894	0.9911	0.17
1	0	1	0	0	3.63E-06	0.9150	0.9071	-0.86
-1	0	1	0	0	5.64E-06	1.4217	1.4311	0.66
0	-1	0	1	0	4.12E-06	1.0391	1.0371	-0.19

Table 8: F_P for RSM for single flap with MH input with 2nd order fit using L_9 OA

x_1	x_2	x_1^2	x_2^2	$x_1 * x_2$	J_P Analysis Prediction	Analysis Dimensionless w.r.t baseline	F_P RSM Prediction (second order fit)	Error b/w RSM (2nd order fit) and Analysis prediction (%)
1	1	1	1	1	9.62E-08	1.5121	1.5078	-0.28
1	-1	1	1	-1	5.28E-08	0.8295	0.8825	6.39
-1	-1	1	1	1	3.169E-08	0.4980	0.5008	0.57
-1	1	1	1	-1	6.11E-08	0.9599	1.0252	6.80
0	0	0	0	0	6.36E-08	1.0000	0.997	-0.30
0	1	0	1	0	8.34E-08	1.3107	1.3396	2.21
1	0	1	0	0	7.18E-08	1.1287	1.1400	1.00
-1	0	1	0	0	4.557E-08	0.7161	0.7079	-1.14
0	-1	0	1	0	4.65E-08	0.7307	0.7647	4.66

Table 9: F_v for RSM for dual flap with MH input with 2nd order fit using L_9 OA

y_1	y_2	y_1^2	y_2^2	$y_1 * y_2$	J_v Analysis Prediction	Analysis Dimensionless w.r.t baseline	F_v RSM Prediction (second order fit)	Error b/w RSM (2nd order fit) and Analysis prediction (%)
1	1	1	1	1	3.55E-06	0.9021	0.9118	1.07
1	-1	1	1	-1	3.60E-06	0.9151	0.9605	4.96
-1	-1	1	1	1	5.46E-06	1.3877	1.3776	-0.73
-1	1	1	1	-1	4.79E-06	1.2166	1.2618	3.71
0	0	0	0	0	3.93E-06	1.0000	0.9992	-0.08
0	1	0	1	0	3.87E-06	0.9842	0.9976	1.36
1	0	1	0	0	3.56E-06	0.9062	0.8966	-1.06
-1	0	1	0	0	4.99E-06	1.2698	1.2802	0.82
0	-1	0	1	0	4.12E-06	1.0470	1.0799	3.14

Table 10: F_P for RSM for dual flap with MH input with 2nd order fit using L_9 OA

y_1	y_2	y_1^2	y_2^2	$y_1 * y_2$	J_P Analysis Prediction	Analysis Dimensionless w.r.t baseline	F_P RSM Prediction (second order fit)	Error b/w RSM (2nd order fit) and Analysis prediction (%)
1	1	1	1	1	1.10E-07	1.6016	1.5838	-1.11
1	-1	1	1	-1	5.50E-08	0.8014	0.8326	3.90
-1	-1	1	1	1	3.98E-08	0.5794	0.5934	2.41
-1	1	1	1	-1	7.76E-08	1.1303	1.169	3.43
0	0	0	0	0	6.86E-08	1.0000	0.9923	-0.77
0	1	0	1	0	9.28E-08	1.3519	1.3863	2.54
1	0	1	0	0	7.70E-08	1.1224	1.1459	2.09
-1	0	1	0	0	5.73E-08	0.8346	0.8188	-1.89
0	-1	0	1	0	4.89E-08	0.7128	0.7229	1.42

Optimal control algorithm discussed in section 3 is used to minimize the vibration objective function and flap actuation power requirement. Response surfaces for F_v and F_P are shown in Figure 3 for single flap case.

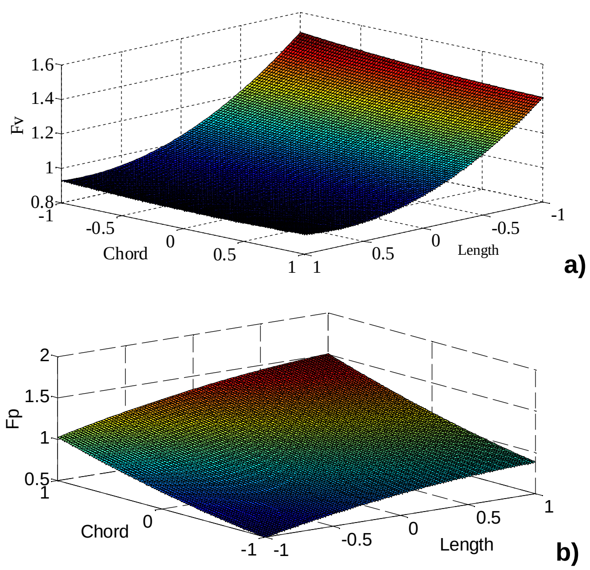

Figure 3. Variation in objective functions for trailing edge flap length and chord dimensions in design space for single flap configuration **a)** F_v **b)** F_P .

Figures 3a and 4a illustrates that flap length is the dominant parameter to minimize F_v; this is also evident from the expression for the objective function in eq. 29 for F_v. The coefficient of the flap length parameter (x_1) is one order of magnitude higher than the flap chord parameter (x_2).

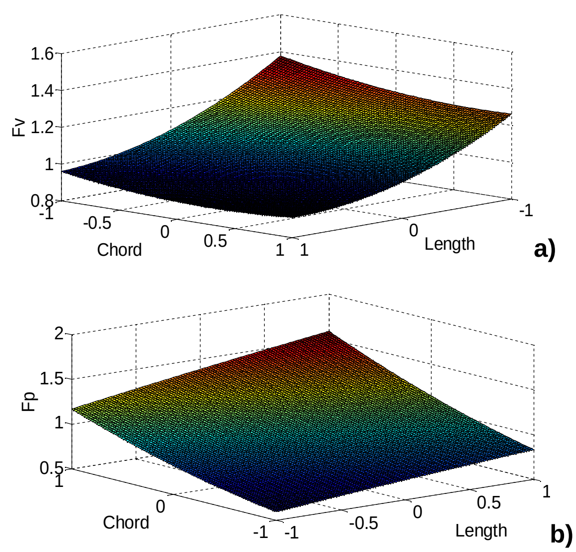

Figure 4. Variation in objective functions for trailing edge flap length and chord dimensions in design space for dual flap configuration **a)** F_v **b)** F_P .

It is apparent from Figures 3a and 4a that F_v is lesser for dual flap configuration than single flap. Figures 3b and 4b depict the variation of response surface for F_P for the single and dual flap cases, respectively. Here, the variation is dominated by the chord length. Since both the objectives posses conflicting nature towards design variables. Therefore, to find the best design point a Pareto optimal design approach is performed. Figure 5 shows a Pareto surface for single trailing edge flap with F_v and F_P as conflicting objective functions. Here the Pareto surface is generated by combining the Figures 3a and 3b. As it is evident from Figure 5, there are two points of interest, point A and point B, which represents design points for minimum vibration levels and minimum flap actuation power, respectively.

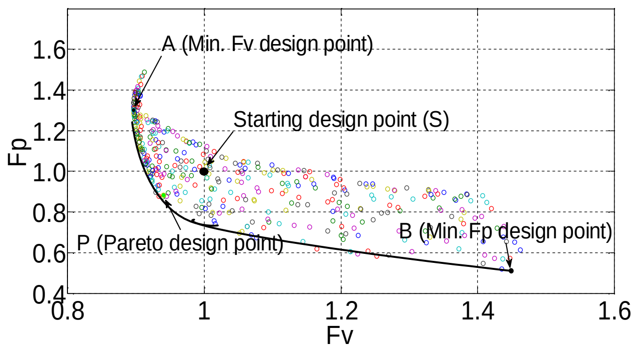

Figure 5. Pareto surface for single flap case

In Figures, $F_v = F_P = 1$ represents the starting design point (S). When both objectives are plotted together, they yield a surface in 2D which contains illusive information at the top edge. The detailed upper and lower part of the Pareto surface is shown in Figure 6. A best Pareto optimal design point is chosen among the given discrete design points. In Figure 5, point P represents a Pareto optimal point.

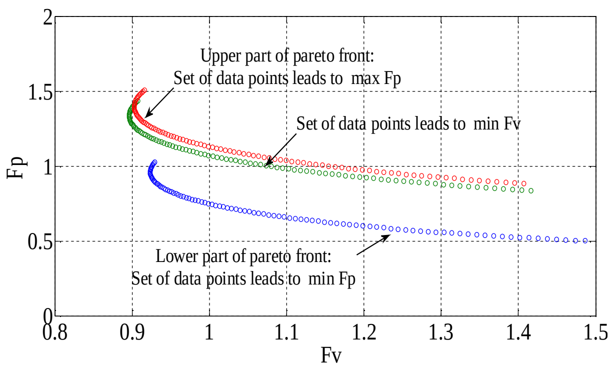

Figure 6. Pareto fronts: single flap, min F_v and F_P

Point A leads to vibration reduction of 71.6% from the baseline case (without flaps), and incurs 51% more flap actuation power than the initial design point S. On the other hand, point B yields vibration reduction of around 54% from the baseline and it requires 50% lesser flap actuation power in comparison to the starting point S. From the Pareto analysis, design point P gives a compromise design between both the objectives. Design point P reduces hub vibration by 71%, which is 2.5% more than the initial design and flap actuation power requirement is reduced by 17% from the starting design (S).

Figure 7 shows the Pareto surface for dual flap configuration. Figure 8 illustrates the set of data points which leads to minimum and maximum of the objectives for two flap case. Here again, two interesting point are observed from the pareto analysis as shown in Figure 7. Point A gives minimum vibration levels and reduces the hub loads by 72% from the baseline at the cost of 60% more flap power in comparison to starting design (S). Minimum flap power can be achieved at the design point B which yields around 58% reduction in hub loads and need 42% less flap power relative to starting design.

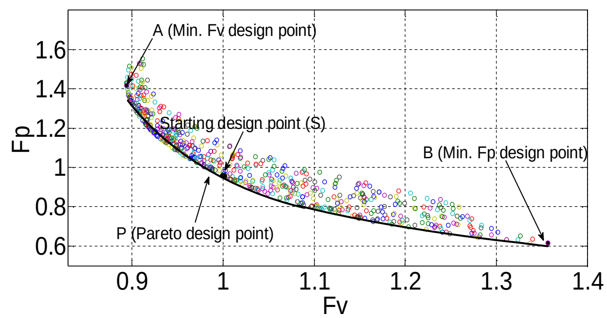

Figure 7. Pareto surface for dual flap configuration

Due to the conflicting nature between the two objectives for the available design points, a Pareto optimal point (P) is selected from the Pareto curve. It suppresses the vibratory loads by 71.7% from baseline case and is around 3% more than the starting design S and requires 20% less flap actuation power. Flap spanwise and chordwise dimensions for single and dual TEF at starting point (S) and Pareto optimal point (P) are shown in Figures 9 and 10, respectively.

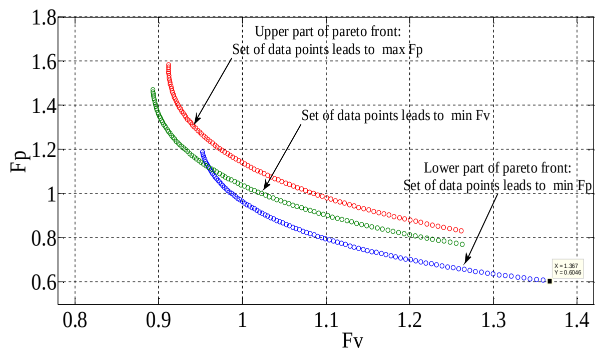

Figure 8. Pareto front: dual flap, min. F_v and F_P

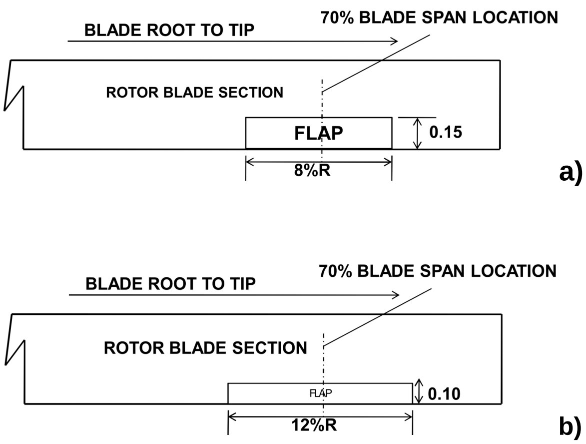

Figure 9. Schematic of rotor blade with single TEF **a)** Starting design (S) **b)** Optimal design (P)

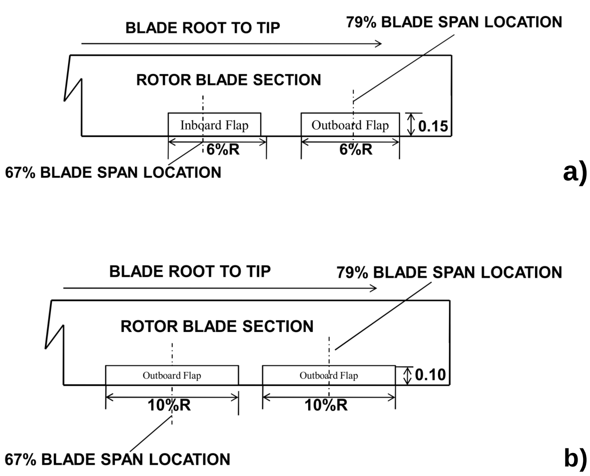

Figure 10. Schematic of rotor blade with dual TEF **a)** Starting design (S) **b)** Optimal design (P)

The detailed comparison of single and dual flap configurations for two different objectives at design points S, A, B and P are shown in Figures 11 and 12, respectively. Here point S represents starting design point and two interesting design points A and B are found along with a Pareto optimal point P, from the set of design points which collectively constitutes the pareto front. Here design point B could be an attractive choice for all practical purposes, as flap power requirement is minimal along with suitable reduction in vibration levels.

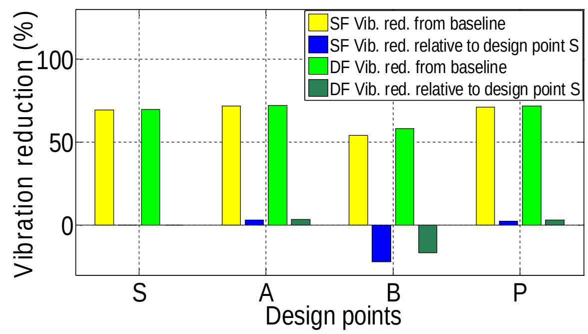

Figure 11. Vibration reduction for single flap (SF) and dual flap (DF) from baseline case (without flaps) for **a)** Starting design point (S) **b)** Min. F_v design (A) **c)** Min. F_P design (B) and **d)** Pareto optimal point (P).

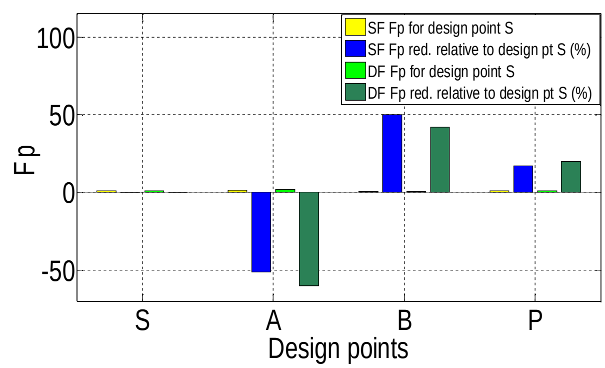

Figure 12. F_P for single flap (SF) and dual flap (DF) for **a)** Starting design point (S) **b)** Min. F_v design (A) **c)** Min. F_P design (B) and **d)** Pareto optimal point (P).

The starting design point (S) chosen here, itself gives adequate vibration reduction from the baseline case (w/o flaps). Nevertheless, the optimal design points obtained using response surface method with OA leads to a robust design with a nominal vibration reduction and reduces flap actuation power around 34% and 40% in comparison to minimum vibration design point (A) for single and dual flap case, respectively.

8. CONCLUSIONS

In this investigation, an optimal single and dual flap designs are obtained which needs less flap actuation power and yields considerable reduction in hub vibration. Aeroelastic analysis is computationally expensive to cascade with conventional optimization algorithms. Response surfaces using orthogonal arrays are used for metamodel development. Flap chord and flap length are the design variables with an objective to simultaneously minimize the hub vibration loads and flap actuation power. Numerical results are obtained for a 4-bladed hingeless helicopter rotor similar to BO105. Following conclusions can be drawn from this study:

1) Orthogonal array inspired response surfaces requires less number of design experiments. Second order polynomial response surfaces adequately approximate the hub vibration levels and flap actuation power. Maximum variation in response surface and aeroelastic analysis prediction is around 5% for F_v and 7% for F_P .

2) Minimum hub vibration levels are obtained for design point A, which suggests to use maximum flap length and chord size for both single and dual flap configurations. Penalty is incurred on the flap actuation power for design point A, as larger flap dimensions requires higher hinge moments, therefore needs more power. Minimum F_v design is sensitive to flap lengths.

3) Design point B leads to minimum F_P for single and dual flap case. It suggests to use smaller flaps for lesser flap actuation power requirement. Minimum F_P point B requires around 50% and 42% less flap power in comparison to starting point (S) for single and dual flap case, respectively.

4) A Pareto front is constructed to obtain the best compromise design. Design point P represents a Pareto optimal point. It minimizes hub vibrations and requires around 20% less flap power than the initial design.

It can be inferred from this study that OA inspired response surface methods can be used to build accurate metamodels to replace the expensive analysis code for robust design of low vibration and flap actuation power trailing edge flap.

REFERENCES

[1] R. G. Loewy, “Helicopter Vibrations: A Technological Perspective,” *Journal of the American Helicopter Society*, Vol. 29, 1984, pp. 4-30.

[2] Wayne Johnson, “Helicopter Theory”, Princeton University. Press, *1980*.

[3] G. Riechert, “Helicopter vibration control-A survey,” *Vertica*, Vol. 5, No. 1, 1981, pp. 1-20.

[4] P. P. Friedmann, and T. A. Millott, “Vibration reduction in rotorcraft using active Control: A comparison of various approaches,” *Journal of Guidance, Control, and Dynamics*, Vol. 18, No. 4, 1995, pp. 664-673.

[5] I. Chopra, “Review of state-of-art of smart structures and integrated systems,” *AIAA Journal,* Vol. 40. No. 11, 2002, pp. 2145-2187.

[6] I. G. Lim and I. Lee, “Aeroelastic analysis of rotor systems using trailing edge flaps”. *Journal of Sound and vibration*, Vol. 321, No. 3-5, 2009, pp. 525–536.

[7] J. Milgram, I. Chopra, and F. Straub, “Rotors with trailing edge flaps: Analysis and comparison with experimental data”, *Journal of the American Helicopter Society*, Vol. 43, No. 4, 1998, pp. 319-332.

[8] M. Fulton, R. Ormiston, "Small-scale rotor experiments with on-blade elevons to reduce blade vibratory loads in forward flight" *In Proceedings of the AHS 54th Annual Forum of the American Helicopter Society, Washington, DC*, 1998, pp. 433–451.

[9] F. K. Straub, V. R. Anand, T. S. Birchette and B. H. Lau, “Wind tunnel test of the SMART active flap rotor,” *In Proceedings of the AHS 65th Annual Forum of the American Helicopter Society*, Grapevine, TX, 2009.

[10] P. Konstanzer, B. Enenkl, P.-A. Aubourg and P. Cranga, "Recent advances in Eurocopter's passive and active vibration control", *In Proceedings of the AHS 64th Annual Forum of the American Helicopter Society, Montréal, Canada, 2008.*

[11] P. Leconte and H. M. des. Rochettes, “Experimental assessment of an active flap device”, *In Proceedings of the AHS 58th Annual Forum of the American Helicopter Society*, Montreal, Canada, 2002.

[12] R. Mallick, R. Ganguli and M. S. Bhat, “An experimental and numerical study of piezoceramic actuator hysteresis in helicopter vibration control using trailing edge flaps”, *Journal of Aerospace: Part G, DOI: 10.1177/0954410013478254, 2013.*

[13] S. R Viswamurthy and R. Ganguli, “An optimization approach to vibration reduction in helicopter rotors with multiple active trailing

edge flaps", *Aerospace Science and Technology*, Vol. 8, No. 3, 2004, pp. 185-194.

[14] R. Mallick, R. Ganguli, M. S. Bhat, "Parametric study of single and dual trailing edge flaps for helicopter vibration reduction", *1st Asian Australian Rotorcraft Forum and Exhibition*, Busan, Korea, 12-15 February 2012.

[15] R. Celi and P. P. Friedmann, "Structural optimization with aeroelastic constraints of rotor blades with straight and swept tips," *AIAA Journal*, Vol. 28, No, 3, 1990, pp. 928-936.

[16] A. Chattopadhyay and T. R. McCarthy, "A multidisciplinary optimization approach for vibration reduction in helicopter rotor blade design," *Computer and Mathematics with Applications*, Vol. 25, No. 2, 1993, pp. 59-72.

[17] C. Venkatesan, P. P. Friedmann and K. A. Yuan, "A new sensitivity analysis for structural optimization of composite rotor blades," *Mathematical and Computer Modeling*, Vol. 19, No. 3-4, 1994, pp. 1-25.

[18] R. Ganguli and I. Chopra, "Aeroelastic optimization of an advanced geometry rotor," *Journal of the American Helicopter Society*, Vol. 41, No. 1, 1996, pp. 18-28.

[19] P. P. Friedmann and P. Shanthakumaran, "Optimum design for rotor blades for vibration reduction in forward fight," *Journal of the American Helicopter Society*, Vol. 29, No. 4, 1984, pp. 70-80.

[20] R. Ganguli and I. Chopra, "Aeroelastic optimization of a helicopter rotor with composite coupling," *Journal of Aircraft*, Vol. 32, No. 6, 1995, pp. 1326–1334.

[21] R. Ganguli, "A survey of recent developments in rotorcraft design optimization", *Journal of Aircraft*, Vol. 41, No. 3, 2004, pp. 493-510.

[22] B. Glaz, P. P. Friedmann and L. Liu, "Surrogate based optimization of helicopter rotor blades for vibration reduction in forward flight" *Structural and Multidisciplinary Optimization*, Vol. 35, No. 4, 2008, pp. 341-363.

[23] T. W. Simpson, J. Peplinski, P. N. Koch and J. Allen, "Metamodels for computer based engineering design: survey and recommendations," *Engineering with Computers*, Vol. 17, No. 2, 2001, pp. 129-152.

[24] J. Sobieszczanski-Sobieski and R. T. Haftka, "Multidisciplinary aerospace design optimization: Survey of recent developments", Structural optimization, Vol. 14, No. 1, 1997, 1-23.

[25] G. Venter and R. T. Haftka, "Construction of response surface approximations for design optimization," *AIAA Journal*, Vol. 36, No. 12, 1998, pp. 2242-2249.

[26] R. Unal, R. D. Braun, A. A. Moore and R. A. Lepsch, "Response surface model building using orthogonal arrays for computer experiments," *19th Annual International Conference of the International Society of Parametric Analysis*, New Orleans, LA, 1997, pp. 469-481.

[27] S. Bhadra and R. Ganguli, "Aeroelastic optimization of a helicopter rotor using orthogonal array based metamodels" *AIAA Journal*, Vol. 44, No. 9, 2006, pp. 1941-1951.

[28] R. H. Myers and D. C. Montgomery, "Response Surface Methodology-Process and Product Optimization Using Designed Experiments", Wiley, New York, 1995.

[29] K. K. Saijal, S. R. Viswamurthy and R. Ganguli, "Optimization of helicopter rotor using polynomial and neural network metamodels", *Journal of Aircraft*, Vol. 48, No. 2, 2011, pp. 553-566.

[30] S. R. Viswamurthy and R. Ganguli, "Optimal placement of trailing edge flaps for helicopter vibration reduction using response surface methods", *Engineering Optimization*, Vol. 39, No. 2, 2007, pp. 185-202.

[31] R. Ganguli, "Optimum design of a helicopter rotor for low vibration using aeroelastic analysis and response surface methods", *Journal of Sound and Vibration*, Vol. 258, No. 2, 2002, pp. 327-344.

[32] I. H., Ibrahim, E. Y. K. Ng, and K. W. L. Wong, "Applying Taguchi's off-line quality control method and ANOVA on the maneuverability of the F-5E intake", *Mathematical and Computer Modelling*, Vol. 49, No. 7–8, 2009, pp. 1359-1371.

[33] Y. Hu and S. S. Rao, "Robust design of horizontal axis wind turbines using Taguchi method", *Journal of Mechanical Design,* Vol. 133, No.11, 2011, pp. 111009.1-111009.15.

[34] P. Chiang and M. R. Chen, "Device optimization using response surface methodology with orthogonal arrays", In Statistical Methodology, IEEE International Workshop on, 2001 6yh, 2001, pp. 17-20.

[35] G. Bir, I. Chopra, R. Ganguli, E. Smith, J. Wang, K. Kim, W. Chan, M. Nixon, N. Kimata, and K. Nguyen, "University of Maryland

advanced rotorcraft code (UMARC) manual", UM-AERO Report, 1994.

[36] N. Hariharan and J. G. Leishman, "Unsteady aerodynamics of a flapped airfoil in subsonic flow by indicial concepts", *Journal of Aircraft*, Vol. 33, No. 5, 1996, pp. 855-868.

[37] R. Ganguli, I. Chopra and W. H. Weller, "Comparison of calculated vibratory rotor hub loads with experimental data", *Journal of the American Helicopter Society,* Vol. 43, No.4, 1998, pp. 312- 318.

[38] M. S. Torok and I. Chopra, "Rotor loads prediction utilizing a coupled aeroelastic analysis with refined aerodynamic modeling", *Journal of the American Helicopter Society,* Vol. 36, No. 1, 1991, pp. 58-67.

[39] W. Johnson, "Self-tuning regulators for multicyclic control of helicopter vibration". *NASA Technical Paper*, 1996.

[40] R. Ganguli, "Engineering Optimization: A modern approach", Universities Press, 2012.

[41] R. Roy, "*A primer on the Taguchi method"*, SME, 2010.

[42] P. J. Ross, "Taguchi techniques for quality engineering", Mcgraw-Hill International editions, New York, 1996.